ACS APPLIED MATERIALS & INTERFACES

Research Article

www.acsami.org

# Crossing the Traditional Boundaries: Salen-Based Schiff Bases for Thermal Protective Applications

Anil D. Naik, Gaëlle Fontaine, Séverine Bellayer, and Serge Bourbigot*

ISP/UMET−UMR/CNRS 8207, Ecole Nationale Supérieure de Chimie de Lille (ENSCL), Avenue Dimitri Mendeleïev−Bât. C7a, BP 90108, 59652, Villeneuve d'Ascq Cedex, France

Supporting Information

**ABSTRACT:** A broad spectrum of applications of "Salen"-based Schiff bases tagged them as versatile multifunctional materials. However, their applicability is often bounded by a temperature threshold and, thus, they have rarely been used for high temperature applications. Our investigation of a classical Schiff base, *N*,*N*′-bis(4-hydroxysalicylidene)-ethylenediamine (L2), reveals that it displays an intriguingly combative response to an elevated temperature/fire scenario. L2 resists and regulates thermal degradation by forming an ablative surface, and acts as a thermal shield. A polycondensation via covalent cross-linking, which forms a hyperbranched cross-linked resin is found to constitute the origin of the ablative surface. This is a unique example of a resin formation produced with a Schiff base, that mimicks the operational strategy of a high-heat resistant phenolic resin. Further applicability of L2, as a flame retardant, was tested in an engineering polymer, polyamide-6. It was found that it reinforces the polymer against fire risks by the formation of an intumescent coating. This paves the way for a new strategic avenue in safeguarding polymeric materials toward fire risks. Further, this material represents a promising start for thermal protective applications.

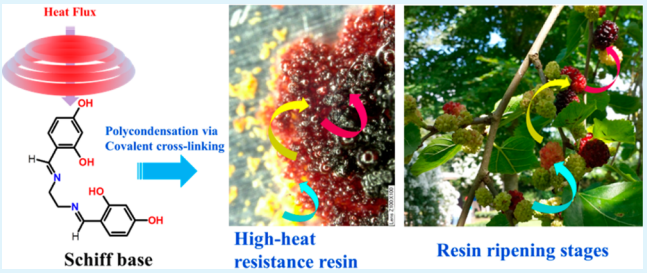


**KEYWORDS:** *Schiff base, Salen, Resorcinol, Phenolic resin, Flame retardancy, Polymers*

## INTRODUCTION

Ever since their discovery, Schiff bases have been subject to rich structural diversification and application proliferation.[1−8] Schiff bases, either alone or in metal-chelated form, find extensive applications in drug discovery, as nonlinear optical materials, in electrochemical cells, as corrosion inhibitors, in gas separation-storage, as molecular sensors/photonic devices, as magnetic materials, as thermo/photochromic materials, etc., and their structure−property relationship is well-documented. They are also being considered as potential candidates in the petroleum and dye industries. However, because of their "soft" molecular network, they have been rarely used for high-temperature thermal protective applications, such as flame retardancy[9] or as ablative materials, which are vital components for contemporary engineering materials.

An ablative surface is a heat shield, which is designed to wear away in a controlled fashion at very high temperature and is mostly used in aerospace applications. Such surfaces are classified according to their dominant ablation process: subliming or melting ablators; charring ablators and intumescent ablators.[10] Thermophysically, this process involves the elimination of a large amount of thermal energy by the sacrifice of the surface material.[10] On the other hand, flame retardants (FRs) are synthetic/natural chemical species incorporated into (or coated onto) polymers to resist ignition/fire, check fire propagation and lessen the consequences of fire hazards.[11] Imparting flame retardancy in engineering polymers has become a necessity and an obligatory based on safety and regulatory issues, respectively.[11,12] FRs are capable of functioning both in gas and condensed phases. Intumescence/char formation in the condensed phase is a physicochemical phenomenon involving formation of a highly cross-linked, swelled carbonaceous material that protects the polymer in several ways.[11] FRs could also work in gas phase thanks to the following contributions: cooling effect, dilution of flammable gases, and radical quenching.

Recently and for the first time, a member of the Schiff base family, the "Salen", was introduced as the base for a new class of flame retardant (FR) and tested in thermoplastic polyurethane.[9] However, the protective process of "Salen" has not been explored. Among these molecules hydroxy-substituted "Salen" Schiff bases (L2 and L3, Figure 1a) were of particular interest. It is because the resorcinol or hydroquinone components of these molecules are known to have extraordinary ability to cross-link (under suitable conditions) and have also been found to be involved in radical chemistry.[13−16] Such properties are attractive to obtain flame retardant properties. With an incentive to provide an insight of their mode of action, and to establish a practical applicability of this "Salen" family in thermal protective applications, the thermal

Received: June 12, 2015
Accepted: September 8, 2015
Published: September 8, 2015




DOI: 10.1021/acsami.5b05164
ACS Appl. Mater. Interfaces 2015, 7, 21208−21217

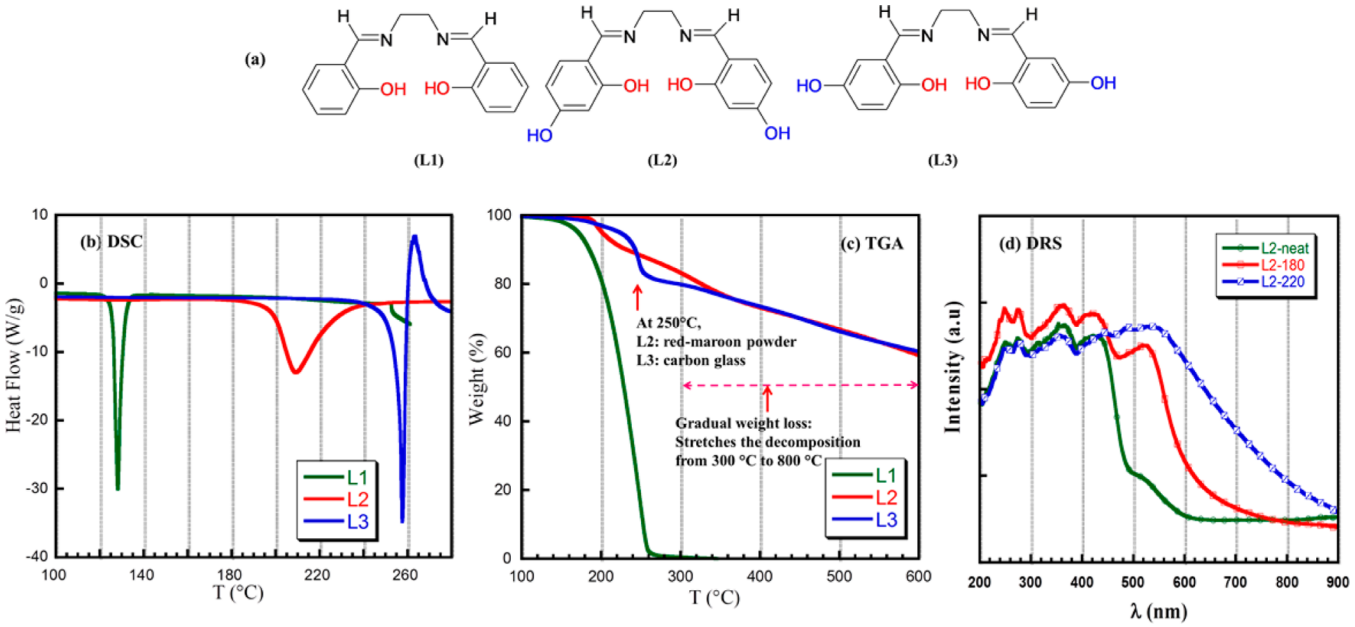


**Figure 1.** (a) Salen-based Schiff bases (L1−L3) synthesized in this study. (b) DSC profiles of L1−L3. (c) TGA profiles of L1−L3 (d) DRS spectra of L2 treated at 180 and 220 °C.

properties of these FRs are probed in the present study. Chronologically, the work reported here starts with an investigation of the thermal degradation of "Salen" covering: the thermal stability, the degradation profile, and the associated structural−chemical−textural transformations. Results will be converged to delineate the thermal protective process. This work is followed by the use of these molecules as potential FR in polyamide-6 (PA 6). The intended proposal to test "Salen" in PA6 is driven by the continuing demand for novel flame retarded PA6 in automotive engineering, electrical/electronics, appliances, building/constructions, etc.[17,18]

Thermal (thermogravimetric analysis, TGA; differential scanning calorimetry, DSC), spectral (diffuse reflectance spectroscopy, DRS; Fourier transform infrared spectroscopy, FTIR; magic angle nuclear magnetic resonance spectroscopy, MAS NMR), microscopic (scanning electron microscope, SEM; electron probe microanalysis, EPMA; optical microscopy) studies were used to investigate the potential intermediates formed during the degradation pathway of L2 in the condensed phase. Volatile components released during the degradation process, which might contribute to gas phase activity, were studied by operand techniques, such as TGA coupled with FTIR (TGA-FTIR), and gas chromatography−mass spectrometry coupled with a pyrolyzer (pyGC/MS). Preliminary results on fire performance and thermal stability of L2 blended PA6 were evaluated with a PCFC (Pyrolysis Combustion flow calorimetry) and a TGA respectively. The PCFC is a suitable tool to study the combustibility/flammability of materials at a small scale.

## 2. EXPERIMENTAL SECTION

*N*,*N*′-Bis(salicylidene)ethylenediamine (L1), *N*,*N*′-bis(4-hydroxysalicylidene)ethylenediamine (L2) and *N*,*N*′-bis(5-hydroxysalicylidene)ethylenediamine (L3) di-Schiff bases were synthesized on the basis of earlier reports (Figure 1a).[9] Samples used for thermal degradation studies were obtained from two methods. First, a controlled heating method was used, which involves heating "Salen" samples in DSC or TGA apparatus under a nitrogen atmosphere (with a heating rate of 10 °C/min) until the desired temperatures. The second thermal treatment method was to place the sample in a ceramic boat and to expose it to a temperature of 800 °C for a short period of time in a preheated furnace. Further information on materials and the instrumental part are given in the Supporting Information.

## 3. RESULTS AND DISCUSSION

**3.1. Thermal Behavior of L1−L3.** L1 is a bright yellow crystalline solid, which shows a sharp melting point at 128 °C during DSC measurements (Figure 1b). Its early decomposition is evidenced from TGA results (Figure 1c). Since L1 is found to have the lowest thermal stability among all, further investigation of this sample is restricted. L2 is a yellow powder with an orange tinge, whereas L3 was isolated as a yellowish-brown crystalline solid.

The color of L2 is sensitive to temperature; it turns orange when the temperature reaches 130 °C. Interestingly this color change is not distinctly reversible. On the other hand, there is also a color change of L3 when heated (yellowish-brown to red), which is clearly reversible. It is well-known that many Salen-based Schiff bases are dimorphic and occasionally the two forms differ in color (yellow or orange-red). These forms are interchangeable with an external perturbation, such as temperature or light irradiation, which are respectively termed as thermochromism or photochromism (Scheme S1).[7] A reversible intramolecular hydrogen atom transfer (keto−enol tautomerism) facilitated by an *o*-hydroxy group is associated with these processes.[7,8,19] The observed distinct reversible color change of L3 is due to thermochromism (thermal response of L3 is dealt separately in section 3.6). However, for L2, the thermochromism process is obscure, because of a differential population of tautomeric species and/or because of a slow fading rate of thermocoloration.[19] Diffuse reflectance spectrum (DRS) measurements of L2 (Figure 1d) at room temperature shows three bands of interests: 350, 425, and a shoulder band at 525 nm. It is reported that for salicylideneanilines, bands in these regions are attributed to enol, *cis*-keto, and *trans*-keto forms, respectively.[7,8]


DOI: 10.1021/acsami.5b05164
ACS Appl. Mater. Interfaces 2015, 7, 21208−21217

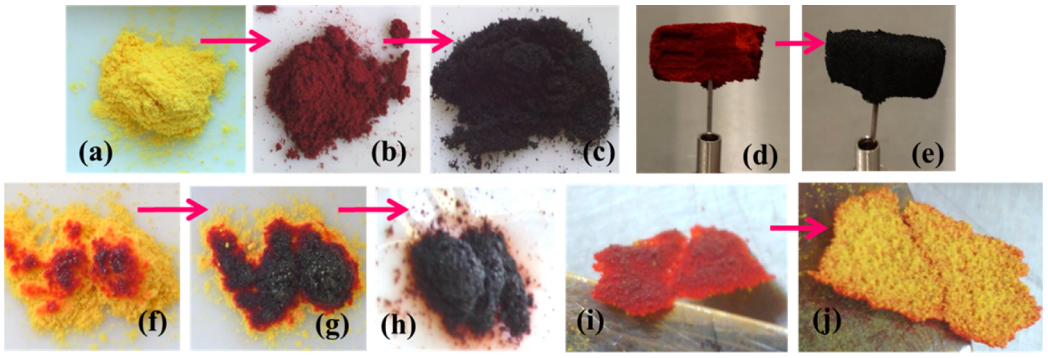


**Figure 2.** (a) L2 powder. (b) L2 heated to 250 °C. (c) L2 heated to 300 °C. (d) L2 heated to 250 °C to obtain a free-standing fused monolith. (e) The same sample heated further to 300 °C. (f) L2 exposed to 800 °C for ∼2s in a furnace. (g) L2 exposed to 800 °C (L2−800) for ∼4 s in a furnace. (h) L2 exposed to 800 °C for ∼10 s in a furnace. (i) Upper fused surface of L2−800. (j) Lower protected surface of L2−800.

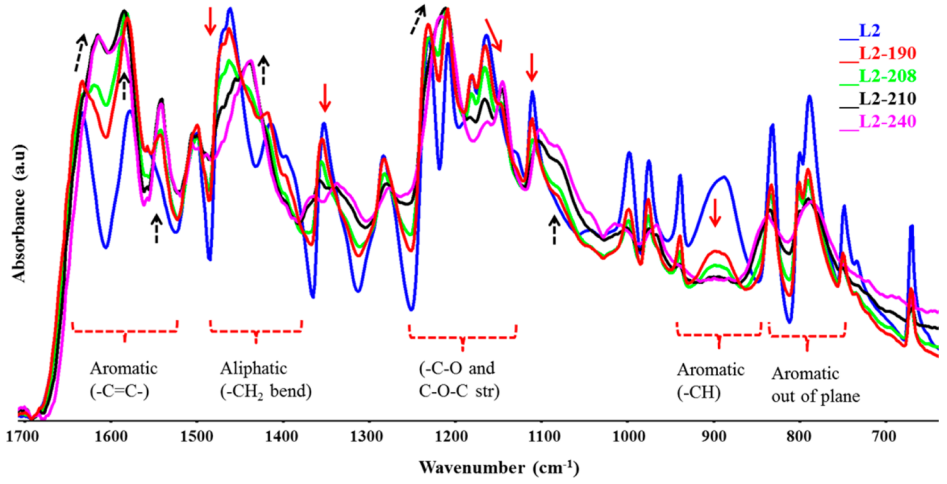


**Figure 3.** FTIR spectra (only expanded region is shown) on thermally treated L2 samples at selected temperatures (Black dotted arrows indicate new bands, red downward arrows indicate decrease/shift of peaks). Tentative regions of concerned IR absorption are also shown.

Further heating of L2 above 130 °C turns its color to orange-red. Hereafter, the color change is distinctly irreversible. When, raising the temperature from 150 °C up to 170 °C deepens this color. TGA, DSC, and FTIR experiments do not show any changes until this temperature. Moreover, no volatile decomposition products are detected during pyGC/MS (desorption method, see the Supporting Information) and TGA-FTIR experiments in this temperature range. Thus, the observed intensification of color of L2 until 170 °C might be due to a structural rearrangement or possibly to a population of stable tautomeric form. Around 180 °C, L2 appears bright red. The DRS spectrum at 180 °C (Figure 1d) shows an intense band around 530 nm. During the first heating ramp of the DSC measurements (Figure 1b), a broad endothermic signal is observed around 210 °C, it does not have any counterpart in the cooling mode and it is absent in the second cycle (not shown). The DRS spectrum at 220 °C (Figure 1c; sample collected after the control heating ramp of the DSC experiment) shows an intense broad band around 530 nm tailing into the visible part of the spectrum. TGA (Figure 1d) indicates an abrupt weight loss step (∼10%) between ∼180 and ∼220 °C. At this temperature, the color of the sample turns to maroon. It is not necessary to heat the sample above 220 °C to achieve this change. Keeping the sample at 160 °C for >1 h brings (maroon-red) color change to the sample. X-ray powder diffraction (XRD) pattern of neat L2 treated at 220 °C indicates (Figure S1) a loss of crystallinity and formation of an amorphous material. After further heating (between 220 and 250 °C), the color changes to reddish-brown, then to brown and finally around 300 °C turns to black solid (Figure 2a−c). It has to be noted that these color changes are highly sensitive to the heating mode and rate, the amount of sample, the uniformity of heating, and its duration. A noticeable feature during the thermal treatment is the progressive gluing of particles. Indeed, a controlled thermal treatment of L2, in a mold, forms a monolith-type material (Figure 2d), which does not collapse when further heating is applied (Figure 2e). This result supports the infusible action and gluing effect. Another significant observation is solubility. L2 is readily soluble in common solvents, but red-maroon powder collected around 220 °C is insoluble even in dimethyl sulfoxide solvent. Unlike L1, which decomposes quite early, the degradation of L2 is very gradual above 250 °C. It is astonishing to note that despite having a simple molecular framework, this molecule stretches its decomposition above 600 °C (Figure 1c). Similar thermal behavior is also observed for L3.

The endothermic irreversible peak seen in the DSC curve, the weight loss step observed in TGA, the distinct color changes, the insolubility in common solvents, the amorphization seen from XRD spectrum and the physical fusion of powder suggest that some chemical/structural changes occur during the thermal treatment of L2 between 180 and 250 °C.


DOI: 10.1021/acsami.5b05164
ACS Appl. Mater. Interfaces 2015, 7, 21208−21217

TGA-FTIR (above 180 °C; not shown) gives an indication that water is evolved at this stage (a band above 3500 $cm^{-1}$ in the FTIR spectrum) and around 200 °C, species having −NH/−OH groups, hydrocarbons, −C−O species (bands: above 3300, 2980−2932, and 1062 $cm^{-1}$, respectively) are detected. Further pyGC/MS experiments confirm that water is evolved around 190 °C and around 200 °C, traces of ethylenediamine (ED) and resorcinol are also identified. Detection of water at this stage may be an indication of some kind of condensation reactions releasing water, rather than a lattice water or water adsorbed at the surface. These preliminary results indicate that there are, indeed, some chemical and structural changes. To track these chemical and structural transformations, L2 was thermally treated at some selected temperatures and studied by FTIR (Figure 3) and solid-state NMR (Figure 4). Results are discussed in the next section.

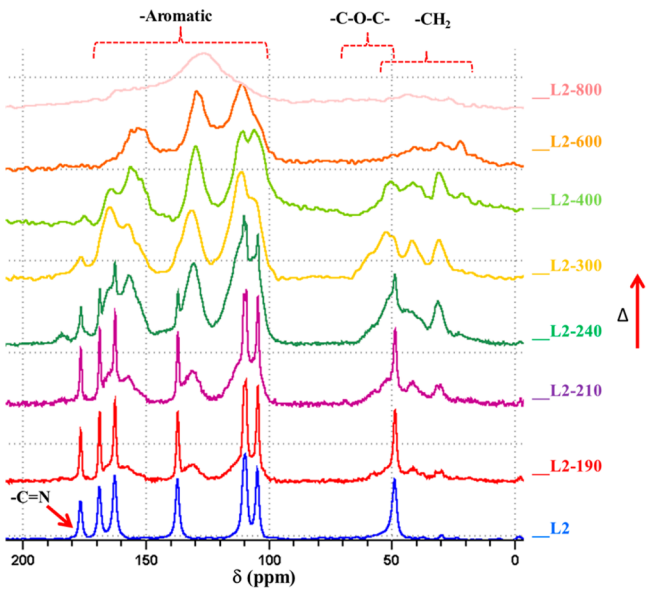


**Figure 4.** $^{13}C$ MAS NMR spectra tracking the structural changes during the thermal treatment of L2 (190−800 indicates the temperature treatment).

The second method of thermal treatment gives additional information. A direct and quick exposure (∼2−3 s) of L2 in an oven at 800 °C imparts bright-red color and, subsequently, the upper surface of the powder fuses to form a protective layer (Figure 2f), which shields the underlying powder (Figure 2j). The fused layer formed (Figure 2f and 2i) is a type of ablative surface, which wears away at higher temperature, protecting the underlying (Figure 2j) material. Longer exposure turns it to black bubbles (Figure 2g), which hardens and finally forms a char (Figure 2h).

**3.2. Probing Chemical Transformations of L2 by FTIR.** Selected FTIR spectra are presented in Figure 3. The number that follows L2 indicates the temperature of treatment. FTIR spectrum of neat L2 shows the following bands (in $cm^{-1}$): 2993br, 2873w from −CH stretch; 1633s is possibly a coupled vibration coming from −C═N and −C═O of a keto form of L2; 1580s, 1553sh, 1500s, for −C═C− ring stretch of aromatic group; 1465s for $-CH_2$ bend of ethylenediamine (ED) component; 1230s, 1210m from −C−O stretch; 1165m from −C−N stretch; 893m from Ar−H wagging; 833m, 790m from out of plane aromatic C−H. The −OH band (4-hydroxy) is not well-defined and a very broad and weak absorption band is observed above 3200 $cm^{-1}$. This is characteristic of a medium strength intermolecular diffuse H-bond, with a large amplitude of the OH vibration or proton transfer equilibrium.[19] The 2-hydroxy group is expected to be locked in a keto−enol tautomerism and may not contribute to the −OH stretching. As the region above 2800 $cm^{-1}$, in the FTIR spectra, is quite broad and not well-defined, we focused our interpretations below 1700 $cm^{-1}$ (Figure 3). The significant changes that took place between 190 and 240 °C are summarized here. With the increase of temperature, new −C═C stretching bands of aromatic ring grow at 1614, 1587, 1542, 1489 $cm^{-1}$ for L2−190. Intensities of these bands increase from L-190 to L2−240 with a slight shift in wavenumber. The existing $-CH_2$ (1465 $cm^{-1}$), which corresponds to $-CH_2$ stretch of ED component, begins to decrease in L2−190 spectrum and a new $-CH_2$ stretching (1438 $cm^{-1}$) band completely replaces this in L2−240 spectrum. As variation in intensity of aromatic −C═C− stretch and $-CH_2$ bending are synchronous, it is reasonable to assume that they are related. These observations suggest the presence of new aromatic (resorcinol or phenolic type) compounds, possibly linked by a $-CH_2$ group. The variation in intensity of aromatic −C═C− stretch indicates varying substitution of aromatic ring and the regions of their presence in the spectrum indicate di, tri-, or tetra substituted aromatic rings.[20−24] Concerned bands in the region between 790 and 900 $cm^{-1}$ also collapses during this thermal treatment, which confirms the substitution of the aromatic/resorcinol ring. Furthermore, in the spectrum, the region 1200−1250 $cm^{-1}$ has undergone several changes too. The −C−O stretch, in L2 spectrum, changes in intensity after heating and is replaced by a broad new band at 1216 $cm^{-1}$in L2−240 spectrum. This new band is, possibly, an ether type bridge (Ar−O−Ar and/or $-CH_2-O-CH_2-$) resulting from the condensation of −OH groups[20−25] on neighboring L2 molecules, which should results in elimination of water molecules (confirmed with pyGC/MS and TGA-FTIR experiments). The −C−N stretch (1165 $cm^{-1}$), in L2 spectrum, also decreases in intensity with temperature (L2−190 spectrum), which is an indication of azomethine breakdown. It continues to reduce in intensity in L2−240 spectrum. This degradation, obviously releases resorcinol (confirmed with pyGC/MS) or resorcinol bearing fragments of azomethine. Thus, FTIR studies confirm Schiff base breakdown, formation of ether bridged, and formation of new methylene-bridged aromatic species.

**3.3. Probing Chemical Transformations of L2 by MAS $^{13}C$ NMR Studies.** The $^{13}C$ MAS NMR study further confirms the formation of new methylene bridged and possibly methylene ether bridges aromatic species. $^{13}C$ NMR of L2 shows the following signals: azomethine at 176 ppm, aromatic carbon atoms between 100 and 170 ppm, and $-CH_2$ carbon at 50 ppm (Figure 4).

NMR of L2−190 shows the presence of additional (weak) set of signals (150−170, 125−135, 110−120 ppm), which correspond to new aromatic carbon species. Their signal intensities progressively increase with the increase of temperature. The other important signals are new aliphatic groups between 29 and 50 ppm and methylene ether bridges around 60 ppm (a weak shoulder), which, like the aromatic signals, progressively increase in intensity.[26−29] It has to be noted that both aliphatic and aromatic signals are broad due to multiple overlapping bands. This is due to the presence of more than one type of $-CH_2$ bridge, on the same aromatic entity or on


DOI: 10.1021/acsami.5b05164
ACS Appl. Mater. Interfaces 2015, 7, 21208−21217

**Scheme 1. Tentative Thermal Protection Pathway Scheme of Salen-Based Schiff Base, L2 (R = remaining part of L2; *o*-QM= *o*-quinone methide)[a]**

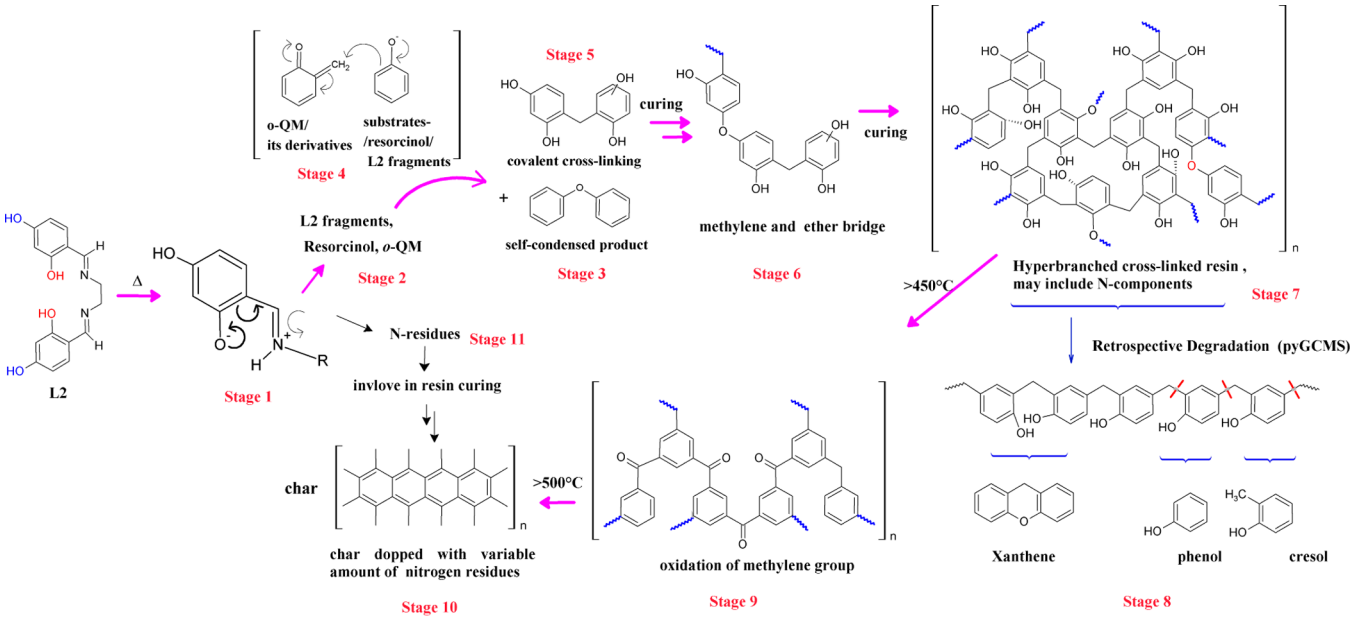


[a]Stages 1−10 correspond to different degradation steps and are discussed in the text.

different aromatic species.[31] L2−400 is a stage of near completion of transformation showing, clearly, a new set of aromatic rings containing $-CH_2$ and −C−O−C components. These results, along with FTIR studies, confirm the chemical transformations and the formation of new species in L2. Above this temperature (>500 °C), ether linkages begin to breakdown and only aliphatic bridges are retained. In L2−600 spectrum, aliphatic signals begin to collapse but aromatic signals (broad peak) are still clearly visible. Finally, L2−800 spectrum shows a broad signal around 125 ppm, which is characteristic of the formation of a char. Thus, NMR witnessed the structural transformations of L2 from powder to the formation of an intumescent structure/char.

**3.4. Electron Probe Microanalysis (EPMA) Studies.** As L2 bear nitrogen atom in its framework, we checked its presence during the whole thermal degradation (on samples shown in Figure 2f−h) by EPMA. It was found that nitrogen is present in variable amount in all the samples (Figure S2). This indicates that nitrogen fragments were carried along during the degradation process until the formation of char. This observation hints to the doping of the intumescent structure by some nitrogenous residues or to the formation of some stable nitrogen species.

**3.5. Structural and Morphological Transformation of L2: An Ablative Intumescence.** On the basis of the above evidence, we are now in position to connect the probable events taking place in the thermal degradation of L2. The broad endotherm observed in the DSC thermogram and the initial small weight loss step in TGA (around 210 °C) are the results of the combinations of several events. We have seen in the previous section that L2 is in a temperature sensitive equilibrium between enol and keto form. Heating L2 provokes population of *cis*-keto and *trans*-keto forms, which is probably a favorable starting point for the cleavage of azomethine linkage after further thermal treatment (Scheme 1, stage 1). The Schiff base break down releases resorcinol, ED and possibly some fragments of L2 (Scheme 1, stage 2). Condensation between some fragmented L2 molecules or non fragmented L2 molecules (via 4-OH groups) releases water molecules. This leads to the formation of new aromatic molecules with ether bridges (Scheme 1, stage 3). During the temperature ramp that cleaves the azomethine group, there is a rearrangement of conjugation on aromatic rings that might produce *o*-quinone methide (*o*-QM)-like species. *o*-QM (Scheme 1, stage 4) is known to be an important intermediate in the poly condensation of resorcinol/phenols and is often known to produce bright colored intermediates.[13,26,28−30] It is also known that resorcinol, either in acidic or basic conditions in the presence of formaldehyde, undergoes self-condensation with the formation of methylene ($-CH_2$) and/or ether bridges (−C−O−C−), and *o*-QM has been suggested to be a transient species. *o*-QM can also reacts with water to form hydroxymethyl molecule, which can favor −C−O−C− linkages. An overview of known reactions involving the poly condensation and the role of *o*-QM is summarized in Scheme S2.

In line with this, it is reasonable to expect that *o*-QM plays a similar role in the formation of observed methylene/methylene ether bridges during L2 degradation (Scheme 1, stage 5). The observed intensification of color during thermal treatment of L2 (to brick red/brown color) is proposed to be due to this *o*-QM reactive species or its derivatives. With further thermal treatment, an initiation of poly condensation is expected among new aromatic molecules and *o*-QM intermediates.[28−30] At higher temperatures, this methylene or ether bridged oligomers (Scheme 1, stage 6) undergo either self-condensation or condensation with other molecules, causing extensive branching/cross-linking and leading to polyaromatic systems (Scheme 1, stage 7). The observed insolubility of L2 at higher temperature is due to this cross-linking.

Retrospective analysis of this condensed pyro-product of L2 provides an indirect evidence of cross-linking phenomenon and positioning of methylene bridges (Scheme 1, stage 8). Following pyrolysis products of polycondensate resins are detected by pyGC/MS (direct pyrolysis, Figure 5): benzene,


DOI: 10.1021/acsami.5b05164
ACS Appl. Mater. Interfaces 2015, 7, 21208−21217

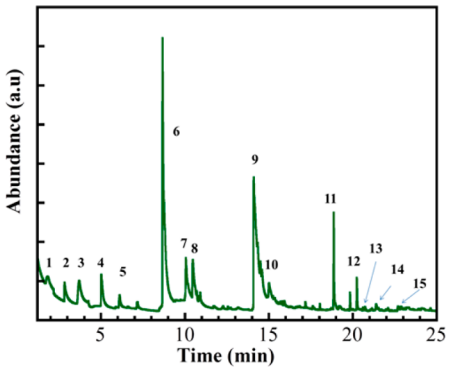


**Figure 5.** Pyrolysis GC/MS chromatogram of L2 pyrolyzed at 600 °C. Identified products are ($m/z$), (1) Benzene (78.1); (2) pyrazine (80.1); (3) toluene (92.1); (4) methyl pyrazine (94.1); (5) xylene (106.2); (6) phenol (94.1); (7) 2-methylphenol (108.1); (8) *p*-cresol (108.1); (9) resorcinol (110.1); (10) 2-methyl hydroquinone (124.2); (11) xanthene (182.2); (12) methylxanthene (192.2); (13) naphthalene (128.2); (14) anthracene (178.2); (15) xanthenone (197.2).

toluene, phenol, methylphenol, polyclic aromatic compounds such as naphthalene, anthracene, xanthenes, which are usual pyro-products of phenolic resins. The scission (300−550 °C) of a terminal benzene ring results in the evolution of phenol or cresol depending on the position of the scission. Formation of xanthene roughly indicates the position of the −OH groups on the phenolic resins formed by an intramolecular cyclization, which forms the ether bridges.

The cross-linked polyaromatic network remains essentially intact until ∼500 °C. The aromatic system is held apart and stabilized by the aliphatic bridges, which ensure that the material does not soften or flow. SEM images show that the clusters of crystals fuse (Figure 6c), swell, and then are transformed into numerous spheres (Figure 6d−f), which are mostly porous.

This process looks similar to an intumescent behavior at the particle level. On the basis of these observations, it can be classified under intumescent ablator. Above 500 °C, a drastic change occurs at the molecular level. The network collapses, aliphatic bridges are destroyed, hydrocarbonaceous residues are eliminated, as shown by NMR and FTIR studies (Figure 4 and Figure S3), and finally, a char of coalesced carbon rings is produced (Figure 2h) (Scheme 1, stage 10), as confirmed by NMR studies. Auto-oxidation of the bridging methylene linkages, as well as the formation of the carbonyl-containing structures (confirmed from FTIR (1750 $cm^{-1}$, Figure S3)) seems to be a step before the char formation (Scheme 1, stage 9). The same sample exposed to a direct high heat flux in a furnace over a period of time also shows the formation of porous spheres, which looks like resin type material under optical microscope (Figure 6g−i). It is concluded that the thermal treatment cures the resin by cross-linking or "thermoset" process and polymerizes the molecules to reach an infusible state. The tightly cured bonding network of aromatic phenolics (or resorcinol) accounts for the cured materials' hardness, low solubility, solvent resistant and observed heat resistant properties. The complete thermosetting resin formation pathway of L2 is outlined in Scheme 1. From the observations and evidence described previously, it can be concluded that these reactions and curing processes of L2 have close resemblance to that of phenolic/resorcinol resins.[30,37−47] Phenolic/resorcinol resins are poly condensation products of phenols/resorcinol and aldehydes and are frequently used as starting materials for the production of chars.[30,31,41,45−50]

Majority of evidence collected so far, during the decomposition of L2, supports the formation of a resin having carbon−oxygen backbone. Hypothetically, there is still a remote scope for another chemical component in this degradation pathway.[32] Although it is obvious that ED of L2 starts to be released quite early, because of the dissociation of the azomethine bond. It is likely that some of the Schiff base molecules remain unaffected and favor the formation of resin-bearing nitrogen components. It is also possible that fragmented nitrogenous residues of L2 may interfere with

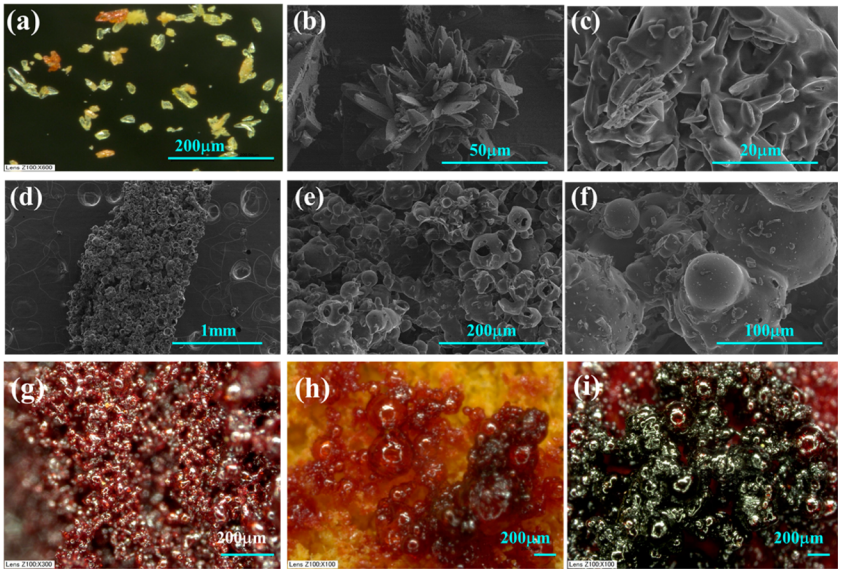


**Figure 6.** (a) Optical microscopic image on single crystals of L2. (b) SEM image on cluster of crystals of L2. (c) SEM image: Effect of thermal treatment (∼200 °C) on clusters. (d−f) SEM images showing formation of resin type material exhibiting an intumescent effect. (g) Optical microscopic image: initial stage of the resin formation (L2 exposed to 800 °C for 2 s in a furnace); (h) optical microscope image: resin ripening (L2 exposed to 800 °C for 4 s in a furnace); (i) optical microscopic image: resin before char formation (L2 exposed to 800 °C for 10 s in a furnace).


DOI: 10.1021/acsami.5b05164
ACS Appl. Mater. Interfaces 2015, 7, 21208−21217

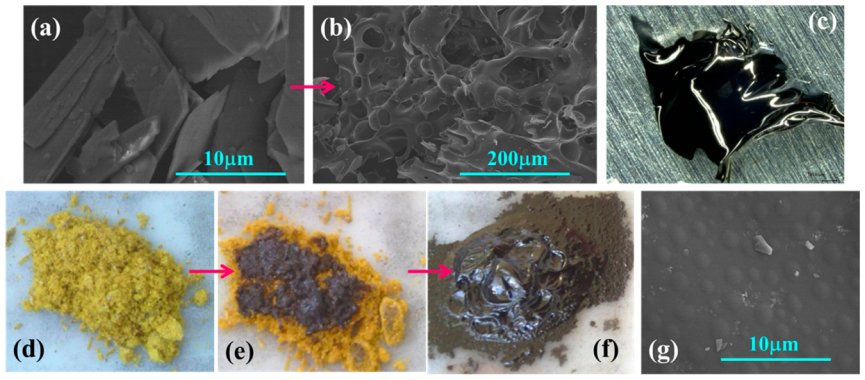


**Figure 7.** Morphological changes of L3 after thermal treatments. (a) SEM image of L3 showing its crystalline nature. (b) SEM image: flat surface of L3 crystals, which starts to coalesce after heating. (c) The reflective and protective surface of the char formed around 250 °C in DSC experiment.(d) Powder sample of L3. (e) L3 after thermal treatment (800 °C in a furnace, 2 s) forms a black protective layer made of bubbles. (f) After further heating, material melts, swells, and forms a protective coating. (g) SEM image on this protective coating showing a pore/crack-free surface.

resorcinol/phenolic curing process, like in the work reported by Solomon and Zhang.[28,33−35] They reported that because of the stability of the benzoxazine-containing[33−35] products, such structures may remain in the resin even under curing condition, inducing the creation of a network built with phenolic rings linked by these N-containing structures, along with methylene bridges.[28] Other nitrogenous residues, such as imines, amides, imides, and benzylamine, were also identified. Polymer frameworks accommodating nitrogen-based pyrrolic and pyridinic-type rings obtained from resorcinol, ED, and formaldehyde are also recently reported.[32] We have seen from EPMA experiments that nitrogen is present in variable amount in all the curing stages. Thus, the formation of nitrogenous residues can be considered as a subsidiary pathway (Scheme 1, stage 11) in the decomposition process of L2, possibly involving resin framework bearing, encompassing benzoxazine fragment[33−36] or other similar nitrogen-containing species.

**3.6. Case Study of L3.** L3 (Figure 1a) having hydroxyl groups on position 2 and 5, exhibits distinct reversible thermochromism (from yellowish-brown at room temperature to red at elevated temperature). Compared to L2, L3 follows a slightly different pathway to form the resin. TGA shows that the weight loss begins a little bit earlier (Figure 1c) than for L2 and forms a plateau after 240 °C, which remains nearly stable until 350 °C. The profile after 350 °C is similar to L2. Under DSC condition, L3 (Figure 1b) does not show any endothermic signal between 180 and 240 °C, unlike L2. FTIR spectra collected at several intervals up to 240 °C, do not show any sign of new species and the color remains the same. However, above 240 °C, L3 abruptly becomes a black powder, and around 260 °C, swells and forms a black reflective layer (Figure 7c). FTIR spectrum shows a drastic change at 250 °C (Figure S4). The region of −OH stretching (3284 $cm^{-1}$), the region around aromatic −C═C− stretch (1485−1635 $cm^{-1}$), the $-CH_2$ stretch of ED (1452 $cm^{-1}$), −C−O (1218 $cm^{-1}$), the aromatic −C−H (around 820 $cm^{-1}$), all have undergone changes. At 260 °C, there is a significant change in the spectral pattern, which indicates the formation of a phenolic resin. The strong band around 1200 $cm^{-1}$ is assigned to the ether bridges between hydroxyl groups of hydroquinone molecules, and 1441 $cm^{-1}$ to the $-CH_2$ bridge between phenyl rings. The asymmetric intensities of −C═C− ring stretch (low intensity at 1590 $cm^{-1}$ and intense signal at 1486 $cm^{-1}$) and the growing band around 810 $cm^{-1}$ strongly support the formation of tetrasubstituted aromatic rings into the formed resin.[42] Figure 7 shows the morphological changes associated with thermal treatment of L3. The L3 powder sample, exposed at 800 °C (for 10 s) in a furnace, turns black, melts to form a compact elastic layer (Figure 7f), which soon swells and finally forms a char. SEM image (Figure 7g) shows the compactness of this char surface, which does not exhibit any cracks.

FTIR spectrum of the melted layer also shows that a resin is formed, stable at high temperature. The observed differences in intensity of the ring −C═C− stretch between L2 and L3, is due to more substituted aromatic rings for L3. Moreover, ether bridge seems to be dominant in L3 (strong band of −C−O−C−). Further $^{13}C$ MAS NMR studies (Figure S5) confirm that, indeed, there is a formation of a new set of aromatic molecules with methylene and/or ether bridges. Further evidence are obtained from pyGC/MS experiements. Molecules like 4,4′-methylenediphenol (with methylene bridge), 4-methoxyphenol (ether bridge), which are part of resin framework, are detected during the degradation of L3. Benzoquinone, which is known for radical scavenging properties is also detected (from pyGCMS studies), indicating the dissociation of azomethine moiety.[15,16] Based on these observations, it can be concluded that the reactivities of L2 and L3 lie in their resin formation pathway and they are most likely to follow Novolac and resol type resin formation, respectively.[30,37] It can be recalled that phenolic resins are classified as novolacs and resols, whereas novolacs and calixresorcinarenes are two well-known derivatives of resorcinol.[30,37,43]

**3.7. L2 as a Flame Retardant in Polyamide-6 (PA6-L2).** The interesting thermal response revealed so far, prompted us to test the efficiency of L2 as FR in polyamide-6 (PA6). L2 is blended with PA6 in a microextruder (see the Supporting Information). The processing temperature of PA6 (255 °C) and the polycondensation temperature regime of L2 coincides and it is reasonable to assume that L2 is no longer in the native L2 form when blended in PA6, but in the more stable and active polycondensed form. In the absence of FRs, PA6 is highly susceptible to fire-risks and burns completely and rapidly in case of fire. A preliminary account of flame retardancy was obtained from PCFC and TGA analysis (Figure S6). Peak of heat release (pHRR) and total heat release (THR) are obtained by evaluating heat release rate (HRR) curve from PCFC, which tentatively determine the fire performances. Neat PA6 shows single-stage HRR curve (peak temperature, 456 °C; pHRR 584 W/g; THR, 29.3 kJ/g). PA6-L2 display nearly the same type of


DOI: 10.1021/acsami.5b05164
ACS Appl. Mater. Interfaces 2015, 7, 21208−21217

HRR curve, but with a slight reduction of pHRR (501 W/g, 14% reduction) and THR values (26.9 kJ/g). From TGA, it can be seen that the degradation of PA6 starts around 350 °C. PA6 undergoes an abrupt and complete decomposition in a single stage without producing any residue. There has been a gradual but continuous weight loss until the onset of the major degradation step of PA6-L2 formulation, which indicates a possible destabilization of polyamide network by L2. Despite this, the formulation undergoes its major decomposition around the same temperature as that of PA6. Unlike neat PA6, the formulation shows 7% (at 450 °C) residue, which indicates the formation of char/intumescent structure. The differences in the thermal decomposition profile between the formulation and neat PA6 points to the deviation in polymer unzipping process. This is due to the interference of the additive in the polymer degradation pathway. Inset of Figure S6 shows an image of the intumescent structure formed when the formulation is exposed to 800 °C in a furnace for 10 s. Under this condition, the formulation initially becomes slightly viscous, then swells, and finally, partly melts. This is associated with a color change to brown. Thereafter, it collapses just to reappear as a shiny swelled porous intumescent structure withstanding the high heat flux.

In the previous section, it is concluded that Salen Schiff base L2 mimics the thermosetting behavior of a resorcinol/phenolic resin, thus promising a pivotal role in flame retardancy. The major flame retardancy action in this Schiff base flame retarded PA6 is shown in the condensed phase (intumescence) via the creation of a resin intermediate, as neat polyamide itself is incapable of building a strong intumescent structure. This swelled char acts as a protective heat shield and slows down the heat/mass transfer between gaseous and condensed phases, limiting the thermo-oxidative degradation of the polymer. It also acts as a protective barrier for the underlying undegraded polymer. It has to be noted that the char formation process and its composition is likely to slightly differ from that of neat L2 because of the polymer matrix effect. Nevertheless, the in situ formation of resorcinol/benzoxazine-based resin is supposed to reinforce PA6 to withstand high temperature by promoting a char formation. It can be expected that the decomposing polyamide matrix fragments can be involved in the cross-linking process of the intumescent structure formation. Because of the deviation in the depolymerization process, the concentrations of flammable polymer fragments are reduced and are rather utilized in cross-linking. In addition, the sublimation tendency of resorcinol might help to obtained a blowing effect.

## CONCLUSIONS

The unique ability of in situ phenolic resin formation in a Schiff base is a new avenue to engineer thermally and chemically resistant FRs and ablative materials. It is noteworthy that the formation of phenolic resin in L2 proceeds in formaldehyde-free media and without supercritical drying condition, it is also an attractive aspect for a low-cost process. The observed polycondensation involves formation of methylenebridges, sandwiched between aromatic rings. Subsequent resin formation and carbonization leads to carbon monoliths. It is the first example of a systematic elucidation of the mode of action of a Schiff base. As cross-linking is an efficient route for intumescence based fire-protections for polymers, these Schiff bases can be flagged as a novel intumescence promoting additives. Moreover, L2 is capable of promoting intumescence in PA6 without the addition of any synergist or acid source. Considering the availability of a wide array of Schiff bases, with easy tailorable framework, further new and exciting properties/materials can be expected. Because Schiff bases have high solubility in common solvents, they can be even easily applied as flame retardant coatings. As the char framework lack inorganic fragments, there are few concerns about the residue recyclability. Melamine, which also has an inherent ability of undergoing polycondensation during thermal treatment, could also be a prospective synergist and can be anchored on Salen framework. Further coupling phenolic resins and usual polymer synergist, such as phosphates and borates, could be promising FR combinations. Poly phenolic resin (as found in case of L2) with a bed of O-donor is an ideal ground for cations (e.g., Zn, Al) and anions (e.g., phosphates) encapsulation for metal-salt based FRs. Finally, formaldehyde-free resin formation, in the present case, could be an incentive for the polyphenol-rich biomass (e.g., Grape sludge, tannins) harvesting for high-temperature applications.

## ASSOCIATED CONTENT

### Supporting Information

The Supporting Information is available free of charge on the ACS Publications website at DOI: 10.1021/acsami.5b05164.

Materials, methods and instrumental part; Scheme of keto−enol tautomerism (Scheme S1); possible polycondensation routes (Scheme S2); XRD of neat L2 and L2 treated at 250 °C (Figure S1); BSE images with corresponding nitrogen detection, (Figure S2); FTIR on residues of L2 at higher temperatures (Figure S3); FTIR of L3 and its thermally treated samples (Figure S4); MAS NMR of L3 and its thermally treated samples (Figure S5); PCFC and TGA results on PA6-L2 (Figure S6) (PDF)

## AUTHOR INFORMATION

### Corresponding Author

*E-mail: serge.bourbigot@ensc-lille.fr.

### Author Contributions

The manuscript was written through contributions of all authors.

### Notes

The authors declare no competing financial interest.

## ACKNOWLEDGMENTS

The authors thank Mr. Bertrand Doumert for his assistance during MAS NMR recording and Mr. Maxence Vandewalle for XRD studies.

## REFERENCES

(1) Calligaris, M.; Randaccio, L..Schiff Bases as Acyclic Polydentate Ligands, In *Comprehensive Coordinate Chemistry*; Wilikinson, G., Gillard, R. D., McCleverty, J. A., Eds.; Pergamon Press, New York, 1987; Vol 2, pp 715−738.

(2) Blagus, A.; Cinčić, D.; Friščić, T.; Kaitner, B.; Stilinović, V. Schiff Bases Derived From Hydroxyaryl Aldehydes: Molecular and Crystal Structure, Tautomerism, Quinoid Effect, Coordination compounds. *Maced. J. Chem. Chem. Eng.* **2010**, *29*, 117−138.

(3) Zhuang, X.; Zhang, F.; Wu, D.; Feng, X. Graphene Coupled Schiff-base Porous Polymers: Towards Nitrogen-enriched Porous Carbon Nanosheets with Ultrahigh Electrochemical Capacity. *Adv. Mater.* **2014**, *26*, 3081−3086.



DOI: 10.1021/acsami.5b05164
*ACS Appl. Mater. Interfaces* 2015, 7, 21208−21217

(4) Vigato, P. A.; Tamburini, S. The Challenge of Cyclic and Acyclic Schiff Bases and Related Derivatives. *Coord. Chem. Rev.* **2004**, *248*, 1717−2128.
(5) Jimenez-Sanchez, A.; Rodrıguez, M.; Metivier, R.; Ramos-Ortız, G.; Maldonado, J. L.; Reboles, N.; Farfan, N.; Nakatani, K.; Santillan, R. Synthesis and Crystal Structures of a Series of Schiff Bases: A Photo-, Solvato- and Acidochromic Compound. *New J. Chem.* **2014**, *38*, 730−738.
(6) Routier, S.; Vezin, H.; Lamour, E.; Bernier, J. L.; Catteau, J. P.; Bailly, C. DNA Cleavage by Hydroxyl-salicylidene-ethylendiamine-iron Complexes. *Nucleic Acids Res.* **1999**, *27*, 4160−4166.
(7) Hadjoudis, E.; Mavridis, I. M. Photochromism and Thermochromism of Schiff Bases in the Solid state: Structural Aspects. *Chem. Soc. Rev.* **2004**, *33*, 579−588.
(8) Chatziefthimiou, S. D.; Lazarou, Y. G.; Hadjoudis, E.; Dziembowska, T.; Mavridis, I. M. Keto Forms of Salicylaldehyde Schiff Bases: Structural and Theoretical Aspects. *J. Phys. Chem. B* **2006**, *110*, 23701−23709.
(9) Fontaine, G.; Turf, T.; Bourbigot, S. Salen Copper Complexes: A Novel Flame Retardant for Thermoplastic Polyurethane. In *Fire and Polymers V*; ACS Symposium Series; American Chemical Society: Washington, D.C., 2009; Vol. *1013*, Chapter 20, pp 329−340.
(10) Favaloro, M. Ablative Materials. *Kirk−Othmer Encyclopedia of Chemical Technology*; John Wiley & Sons: New York, 2000.
(11) Bourbigot, S.; Le Bras, M.; Troitzsch, J. In *Flammability Handbook*;Troitzsch, J., Ed.;Hanser Verlag: Munich, 2003; pp 3−7.
(12) Schartel, B. Phosphorus-based Flame Retardancy Mechanisms-Old Hat or a Starting Point for Future Development? *Materials* **2010**, *3*, 4710−4745.
(13) Durairaj, R. B. *Resorcinol: Chemistry, Technology and Applications*; Springer: New York, 2005.
(14) Pawlowski, K. H.; Schartel, B. Flame Retardancy Mechanisms of Triphenyl Phosphate, Resorcinol bis(diphenyl phosphate) and Bisphenol A bis(diphenyl phosphate) in Polycarbonate/acrylonitrile−butadiene−styrene blends. *Polym. Int.* **2007**, *56*, 1404−1414.
(15) Mikulski, D.; Górniak, R.; Molski, M. A Theoretical Study of the Structure−radical Scavenging Activity of trans-resveratrol Analogues and cis-resveratrol in Gas phase and Water environment. *Eur. J. Med. Chem.* **2010**, *45*, 1015−1027.
(16) Thavasi, V.; Bettens, R. P.; Leong, L. P. Temperature and Solvent Effects on Radical Scavenging Ability of Phenols. *J. Phys. Chem. A* **2009**, *113*, 3068−3077.
(17) Samyn, F.; Bourbigot, S. Protection Mechanism of a Flame-retarded Polyamide 6 Nanocomposite. *J. Fire Sci.* **2014**, *32*, 241−256.
(18) Weil, E. D.; Levchik, S. Current Practice and Recent Commercial Developments in the Flame Retardancy of Polyamides. *J. Fire Sci.* **2004**, *22*, 251−264.
(19) Hadjoudis, E.; Rontoyianni, A.; Ambroziak, K.; Dziembowska, T.; Mavridis, I. M. Photochromism and Thermochromism of Solid trans-N,N′-bis-(salicylidene)-1,2-cyclohexanediamines and trans-N,N′-bis-(2-hydroxy-naphylidene)-1,2-cyclohexanediamine. *J. Photochem. Photobiol., A* **2004**, *162*, 521−530.
(20) Morterra, C.; Low, M. J. The Pyrolysis of a Phenol-formaldehyde Resin. *Carbon* **1985**, *3*, 525−530.
(21) Trick, K. A.; Saliba, T. E. Mechanisms of the Pyrolysis of Phenolic Resin in a Carbon/phenolic Composite. *Carbon* **1995**, *33*, 1509−1515.
(22) Costa, L.; Rossi di Montelera, L.; Camino, G.; Weil, E. D.; Pearce, E. M. Structure-Charring Relationship in Phenolformaldehyde type Resins. *Polym. Degrad. Stab.* **1997**, *56*, 23−35.
(23) Chen, Y.; Chen, Z.; Xiao, S.; Liu, H. A Novel Thermal Degradation Mechanism of Phenol−formaldehyde type Resins. *Thermochim. Acta* **2008**, *476*, 39−43.
(24) Meng, Y.; Gu, D.; Zhang, F.; Shi, Y.; Cheng, L.; Feng, D.; Wu, Z.; Chen, Z.; Wan, Y.; Stein, A.; Zhao, D. A Family of Highly Ordered Mesoporous Polymer Resin and Carbon Structures from Organic−Organic Self-Assembly. *Chem. Mater.* **2006**, *18*, 4447−4664.
(25) Poljanšek, I.; Krajnc, M. Characterization of Phenol-Formaldehyde Prepolymer Resins by In Line FT-IR Spectroscopy. *Acta Chim. Slov.* **2005**, *52*, 238−244.
(26) Mulik, S.; Sotiriou-Leventis, C.; Leventis, N. Electrically Conducting Carbon Networks by Pyrolysis of Isocyanate-Cross-Linked Resorcinol-Formaldehyde Aerogels. *Chem. Mater.* **2008**, *20*, 6985−6997.
(27) Carriazo, D.; Gutiérrez, M. C.; Ferrer, M. L.; del Monte, F. .Resorcinol-Based Deep Eutectic Solvents as Both Carbonaceous Precursors and Templating Agents in the Synthesis of Hierarchical Porous Carbon Monoliths. *Chem. Mater.* **2010**, *22*, 6146−6152.
(28) Zhang, X.; Solomon, D. H. The Chemistry of Novolac resin: 9. Reaction Pathways Studied via Model Systems of ortho-hydroxybenzylamine Intermediates and Phenols. *Polymer* **1998**, *39*, 6153−6162.
(29) Lin-Gibson, S. Cresol Novolac/epoxy Networks: Synthesis, Properties and Processability. Ph.D Thesis, Virginia Polytechnic Institute, Blacksburg, VA, 2001.
(30) Pilato, L. *Phenolic Resins: A Century of Progress*; Springer: Berlin, 2010.
(31) Grenier-Loustalot, M.-F.; Larroque, S.; Grenier, P. Phenolic Resins: 5. Solid-state Physicochemical Study of Resoles with Variable F/P ratios. *Polymer* **1996**, *37*, 639−650.
(32) Wickramaratne, N. P.; Xu, J.; Wang, M.; Zhu, L.; Dai, L.; Jaroniec, M. Nitrogen Enriched Porous Carbon Spheres: Attractive Materials for Supercapacitor Electrodes and $CO_2$ Adsorption. *Chem. Mater.* **2014**, *26*, 2820−2828.
(33) http://www.henkel.com/press/press-releases-2010-20100407-new-resin-technology-for-advanced-composites-25336.htm.
(34) Yagci, Y.; Kiskan, B.; Ghosh, N. N. Recent advancement on Polybenzoxazine-A newly Developed High Performance Thermoset. *J. Polym. Sci., Part A: Polym. Chem.* **2009**, *47*, 5565−5576.
(35) Hao, G.-P.; Li, W.-C.; Qian, D.; Wang, G.-H.; Zhang, W.-P.; Zhang, T.; Wang, A.-Q.; Schüth, F.; Bongard, H.-J.; Lu, A.-H. Structurally Designed Synthesis of Mechanically Stable Poly(benzoxazine-co-resol)-Based Porous Carbon Monoliths and their Application as High-Performance $CO_2$ Capture Sorbents. *J. Am. Chem. Soc.* **2011**, *133*, 11378−11388.
(36) Sevilla, M.; Fuertes, A. B. Fabrication of Porous Carbon Monoliths with a Graphitic Framework. *Carbon* **2013**, *56*, 155−166.
(37) Hesse, W.; Lang, J. Phenolic resins. In *Ullmann's Encyclopedia of Industrial Chemistry*; Wiley−VCH: Weinheim, Germany, 2011.
(38) Muylaert, I.; Verberckmoes, A.; De Decker, J.; Van Der Voort, P. Ordered Mesoporous phenolic resins: Highly Versatile and Ultra Stable Support Materials. *Adv. Colloid Interface Sci.* **2012**, *175*, 39−51.
(39) Manfredi, L. B.; Puglia, D.; Kenny, J. M.; Vazquez, A. Structure-Properties Relationship in Resol/Montmorillonite Nanocomposites. *J. Appl. Polym. Sci.* **2007**, *104*, 3082−3089.
(40) Kim, Y. J.; Kim, M. I.; Yun, C. H.; Chang, J. Y.; Park, C. R.; Inagaki, M. Comparative Study of Carbon Dioxide and Nitrogen Atmospheric Effects on the Chemical Structure Changes During Pyrolysis of phenol−formaldehyde Spheres. *J. Colloid Interface Sci.* **2004**, *274*, 555−562.
(41) Cohen, Y.; Aizenshtat, Z. Investigation of Pyrolytically Produced Condensates of Phenol-Formaldehyde Resins, in relation to their Structure and Decomposition Mechanism. *J. Anal. Appl. Pyrolysis* **1992**, *22*, 153−178.
(42) Fitzer, E.; Schafer, W. The Effect of Crosslinking on the Formation of Glasslike Carbons from Thermosetting Resins. *Carbon* **1970**, *8*, 353−364.
(43) Lee, Y.-K.; Kim, D.-J.; Kim, H.-J.; Hwang, T.-S.; Rafailovich, M.; Sokolov, J. Activation Energy and Curing Behavior of Resol- and Novolac-type Phenolic Resins by Differential Scanning Calorimetry and Thermogravimetric Analysis. *J. Appl. Polym. Sci.* **2003**, *89*, 2589−2596.
(44) Zeng, S.; Guo, L.; Zhang, L.; Cui, F.; Zhou, J.; Gao, Z.; Chen, Y.; Shi, J. Facile Synthesis of Nanoporous Hydroquinone/Catechol Formaldehyde Resins and their Highly Selective, Efficient and


DOI: 10.1021/acsami.5b05164
*ACS Appl. Mater. Interfaces* 2015, 7, 21208−21217

Regenerate Reactive Adsorption for Gold Ions. *Macromol. Chem. Phys.* **2010**, *211*, 845−853.
(45) Pekala, R. W. Organic Aerogels From the Polycondensation of Resorcinol with Formaldehyde. *J. Mater. Sci.* **1989**, *24*, 3221−3227.
(46) Volodko, L. V.; Ostrovskaya, L. E.; Ksenofontov, M. A.; Matusevich, P. A. Structural Changes in the Polycondensation Products of Resorcinol During Heat Treatment. *J. Appl. Spectrosc.* **1972**, *17*, 1613−1615.
(47) Kobayashi, A.; Konishi, G. Synthesis and Analysis of Resorcinol-acetone Copolymer. *Molecules* **2009**, *14*, 364−377.
(48) Allen, D. J.; Ishida, H. Physical and Mechanical Properties of Flexible Polybenzoxazine resins: Effect of Aliphatic Diamine Chain Length. *J. Appl. Polym. Sci.* **2006**, *101*, 2798−2809.
(49) Demetgül, C.; Delikanlı, A.; Sarıbıyık, O. Y.; Karakaplan, M.; Serin, S. Schiff Base Polymers Obtained by Oxidative Polycondensation and Their Co(II), Mn(II) and Ru(III) Complexes: Synthesis, Characterization and Catalytic Activity in Epoxidation of Styrene. *Des. Monomers Polym.* **2012**, *15*, 75−91.
(50) Dilek, D.; Doğan, F.; Bilici, A.; Kaya, I. Oxidative Synthesis of a Novel Polyphenol Having Pendant Schiff Base group: Synthesis, Characterization, Non-isothermal Decomposition Kinetics. *Thermochim. Acta* **2011**, *518*, 72−81.


DOI: 10.1021/acsami.5b05164
*ACS Appl. Mater. Interfaces* 2015, 7, 21208−21217